EPMA-based mass balance method for quantitative fission product distribution comparison between TRISO particles

Wright, Karen E.; Stempien, John D.; van Rooyen, Isabella J.

DOI
10.1557/s43580-021-00166-2

Publication date
2022

Document Version
Final published version

Published in
MRS Advances

MRS Advances (2021) 6:1020–1025
https://doi.org/10.1557/s43580-021-00166-2

ORIGINAL PAPER

EPMA-based mass balance method for quantitative fission product distribution comparison between TRISO particles

Karen E. Wright[1,2] · John D. Stempien[3] · Isabella J. van Rooyen[3]

Received: 25 August 2021 / Accepted: 15 November 2021 / Published online: 3 February 2022

Abstract

Two irradiated AGR-2 TRISO particles were chosen to demonstrate a recently developed mass balance technique in which EPMA-generated concentration data were used to determine fission product mass on a layer-by-layer basis in TRISO particles. EPMA-calculated fission product masses for most fission products in the two particles were within ± 20% of their ORIGEN-modelled masses. Results show that Sr, Ba, and Eu accumulate preferentially in the carbon-rich kernel periphery on the particles' side that lacks a gap between the buffer and IPyC. In addition, the more mobile elements—Cs, Sr, Pd, and Ag, accumulate in greater quantity in the outer layers of particle AGR2-223-RS34 compared to particle AGR2-223-RS06, which has relatively more of those elements' mass located in the kernel and kernel periphery, suggesting enhanced fission product transport in particle AGR2-223-RS34. This model can be used better understand and test fission product transport in TRISO particles.

Introduction

The AGR-2 tristructural isotropic (TRISO)-coated nuclear fuel particle is composed of a UCO fuel kernel 425 µm in diameter in the centre, with concentric outer layers consisting of a 100 µm-thick porous carbon buffer layer, followed by a 40 µm-thick dense inner pyrolytic carbon layer (IPyC) and a 35 µm-thick SiC layer. These layers are overlain by a protective 40 µm-thick outer pyrolytic carbon layer (OPyC) (Fig. 1) [1]. At the time of fabrication the outer portion of the kernel (kernel periphery (KP)) is composed primarily of UO_2 and may have a rind of UC between the KP and the buffer. During irradiation the KP becomes much more C-rich than the inner kernel. Owing to buffer densification during irradiation [2–4], a gap often forms between the buffer and IPyC around part or all of the buffer perimeter (Fig. 1). The KP thickness appears to be asymmetrical with the gap-less side of the particle being thicker than the side with the gap [5].

The objective of this work is to compare the fission product (FP) mass and spatial distribution between two similarly irradiated TRISO particles using a newly developed electron probe microanalysis (EPMA) mass balance method [6] in an effort to gain insight into particle variability within the same compact.

Experiment details

Among the numerous AGR-2 TRISO particles irradiated at Idaho National Laboratory's (INL) Advanced Test Reactor (AGR), two particles were selected from AGR-2 compact 2-2-3 for post-irradiation examination, which included EPMA. Irradiation parameters are shown in Table 1. Details concerning Oak Ridge National Lab's (ORNL) work with compact deconsolidation and TRISO particle sample preparation can be found in [7]. Irradiated microsphere gamma analysis (IMGA) was used to determine the fraction of high-yield isotopes retained in each particle [8]. The ^{110m}Ag measured-to-calculated (M/C) ratio obtained from this analysis was the primary factor for particle selection for scanning microscopy (SEM) analysis [9]. Upon completion of SEM analysis, a subset of particles was sent from ORNL to INL for further analyses. These particular

✉ Karen E. Wright
Karen.Wright@inl.gov

1 Advanced Characterization Department, Idaho National Laboratory, PO Box 1625, Idaho Falls, ID 83415, USA

2 Department of Radiation Science and Technology, Delft University of Technology, Delft, The Netherlands

3 Fuel Development, Performance, and Qualification Department, Idaho National Laboratory, Idaho Falls, ID, USA

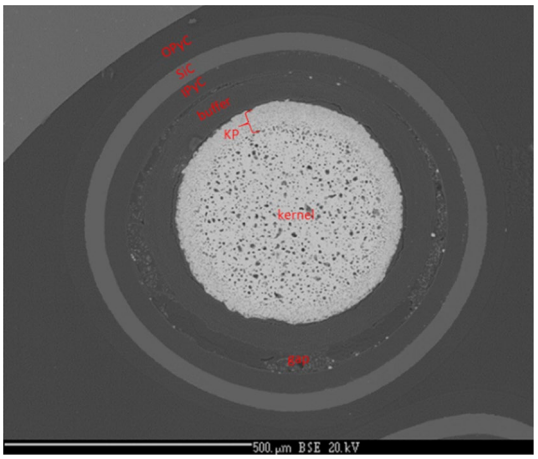

Fig. 1 Shows an irradiated TRISO particle with layers labelled. Note the gap formed between the buffer and IPyC on one side of the particle

particles were chosen for EPMA analysis because although they were irradiated in the same compact and thus under the same conditions, AGR2-223-RS06 retained only ~ 10% of the Ag retained by particle AGR2-223-RS34. As particle temperature is thought to influence strongly Ag retention [10], selection of particles with high and low retained ^{110m}Ag is thought to allow examination of particles with differing temperature histories, despite the particles having the same time-averaged, volume-averaged (TAVA) compact temperature. Recent work by Gerczak et al. [9] suggests that intra-compact temperature variability for AGR-2 particles is on the order of 200 °C; therefore, if elevated temperature is the only driver for Ag loss, particle AGR2-223-RS06 would be expected to have experienced higher temperatures than particle AGR-223-RS34.

An EPMA mass balance method developed by Wright et al. [6] was used to compare the two similarly irradiated particles to determine how FPs distribute differently within two particles irradiated in the same compact. Briefly, U and various FP element concentrations were measured at intervals of 2–5 µm along two radial traverses on each particle. The concentration of a particular element at a particular point was assumed to represent the concentration of that element in an envisioned hemispheric shell with a radius equal to the distance interval along the traverse and a thickness equal to the traverse measurement interval. Using the density of the particle layer, its radial position and the hemispheric shell thickness, the element concentration measured at that radial position was converted to mass, with elemental masses in concentric hemispheric shells added together to arrive at a total particle mass on a layer-by-layer basis. This allowed for total mass comparisons between particles and between the gap and gap-less side of each particle. EPMA-calculated total masses were then compared with ORIGEN modelling to test the accuracy of the EPMA mass balance method.

Results and discussion

EPMA-computed mass balance compared to ORIGEN modelling predictions

Using coupled Monte Carlo N-Particle (MCNP) and Oak Ridge Isotope Generation (ORIGEN) simulations, it is possible to use the ATR irradiation power history to predict compact-level fission product inventory [11]. These inventory values can then be divided by the average number of particles in a compact (~ 3176) to obtain a per-particle inventory estimate. Figure 2a shows the EPMA-computed mass compared with the ORIGEN-predicted mass [11] for particle AGR2-223-RS34, cast as a ratio of the EPMA-calculated mass divided by the ORIGEN-predicted mass. The EPMA-calculated mass is within ± 20% of the ORIGEN-predicted mass for most of the measured elements. Elements with large deviations (> 40%) include Xe, Cd, and Te. The calculated:predicted elemental mass ratios for particle AGR2-223-RS06 are quite similar (Fig. 2b) to those observed in AGR2-223-RS34 (Fig. 2a). Note that the calculated fission product values are not corrected for fission product loss from the particles.

As Xe remains in the gas phase at room temperature, it tends to be lost during sample polishing. Cd is found in trace element quantities and its peak is strongly overlapped by U, which is found in large quantities, making Cd challenging to quantify in the kernel and KP. Elements such as Ag and Sr are somewhat less homogeneously distributed than elements such as the lanthanides and Cs. As a result, calculating masses from only two radial traverses may not capture

Table 1 Shows irradiation parameters for particles AGR2-223-RS34 and AGR2-223-RS06 [11–13]

Parameter	AGR2-223-RS34	AGR2-223-RS06
^{235}U enrichment	14.03	14.03
% FIMA average burnup	10.82	10.82
Time-average, volume average temperature (TAVA), °C	1261	1261
Approximate fast fluence [$E > 0.18$ MeV] ($\times 10^{25}$), n/m^2	2.99	2.99
Measured to calculated ^{110m}Ag ratio	0.84	0.08

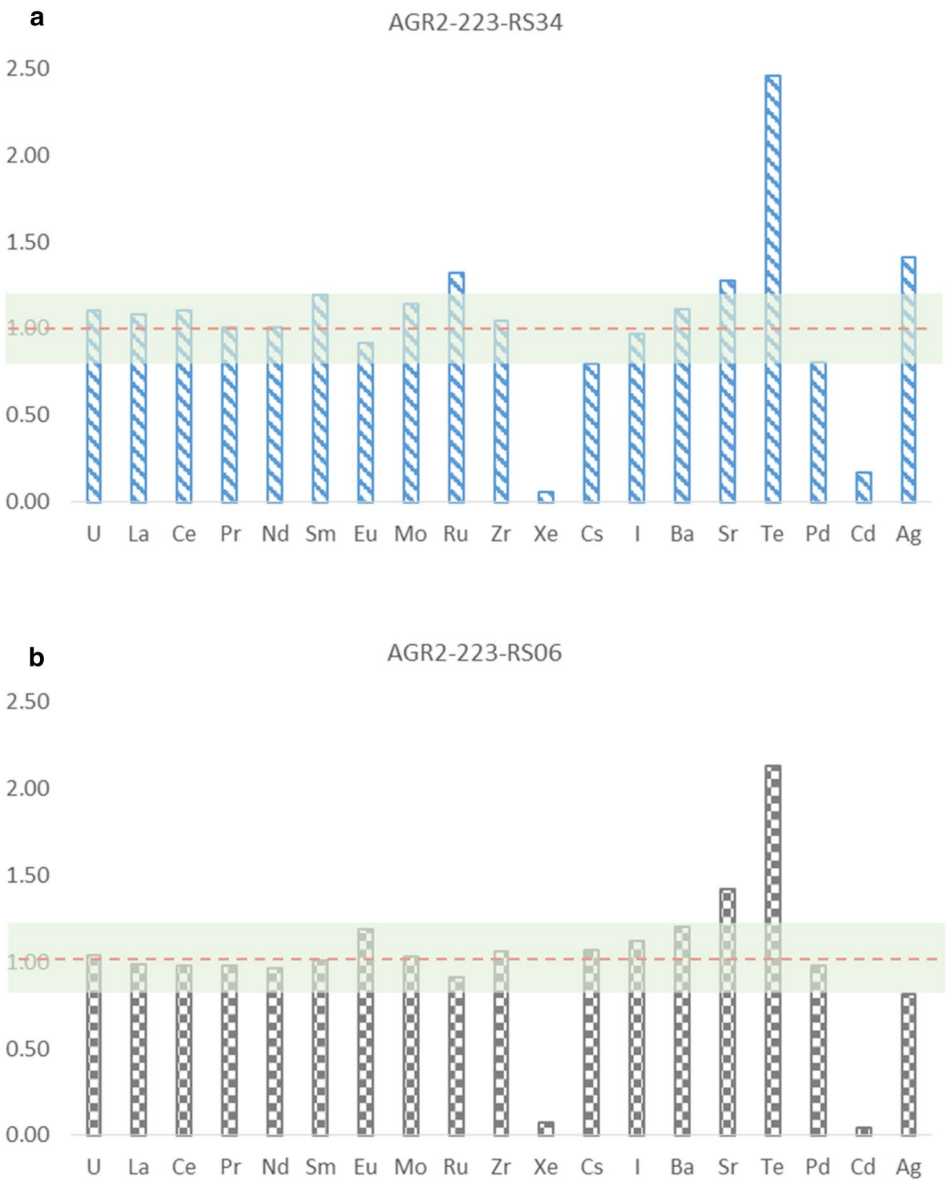

Fig. 2 **a**, **b**. Shows the ratio of the EPMA-calculated particle mass to the ORIGEN-predicted mass for U and 18 FPs in particle AGR2-223-RS34 (**a**) and particle AGR2-223-RS06 (**b**). The horizontal dotted line denotes a 1:1 ratio between calculated and predicted masses while the shaded box indicates the ± 20% calculated:predicted ratio region

adequately the spatial distribution of these elements; nonetheless, Ag and Sr error is < ~40% in these two particles. While Te is also not distributed homogeneously, the source of its large error is uncertain at this time.

Cs, Sr, Pd, Ag, and Ru layer distribution comparison

Figure 3a–e shows the EPMA-calculated masses for individual particle layers in both particles. Figure 3a shows that for particle AGR2-223-RS06, approximately 35% of the Cs mass is retained in the kernel and KP while 65% of the Cs mass is outside of the kernel and KP. In contrast particle AGR2-223-RS34 retains 22% of its Cs mass in the kernel and KP while 78% is outside of those layers. This suggests that Cs transport in particle AGR2-223-RS34 is enhanced relative to that in AGR2-223-RS06.

Figure 3b shows that kernel and KP Sr mass measurements are within the 99% CI error bars for both particles, suggesting no statistical difference between them; however, AGR2-223-RS34 appears to contain slightly more Sr in the buffer, IPyC, and SiC than is present in those regions in particle AGR2-223-RS06, suggesting there is more Sr release from the kernel of AGR2-223-RS34 compared to that of AGR2-223-RS06. Similarly, Fig. 3c, d shows that large Pd and Ag masses remain in the kernel for both particles; however, AGR2-223-RS06 contains about 30% Pd in its kernel and approximately 25% more Ag in its kernel than is observed in AGR2-223-RS34. Moreover, AGR2-223-RS34 contains more Pd and Ag mass outside the kernel compared to AGR2-223-RS06. As particle AGR2-223-RS34 retained ten times more Ag than particle AGR2-223-RS06, the smaller mass of Ag in the outer layers of the latter particle

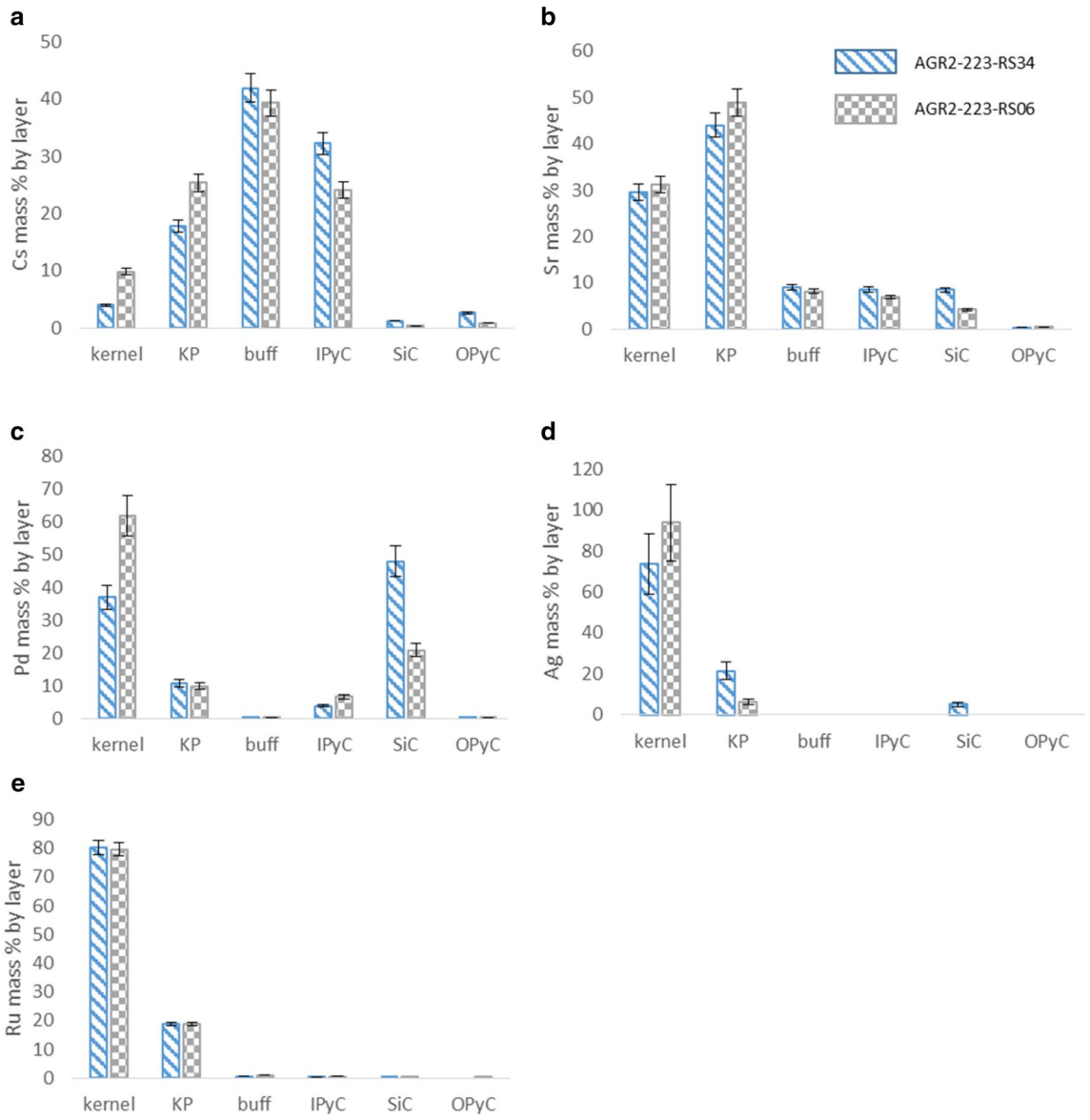

Fig. 3 **a**–**e**. Shows the EPMA-calculated elemental mass as a percentage of the total particle elemental mass for each of the layers in particles AGR2-223-RS34 and ARG2-223-RS06. Elements shown include **a** Cs; **b** Sr; **c** Pd; and **d** Ag; and **e** Ru. 99% confidence interval error bars are shown

may be because most of the Ag had been released. In contrast to Fig. 3a–d, Fig. 3e shows that a less-mobile element such as Ru behaves the similarly in both particles.

Sr accumulation in the TRISO layers in the gap versus gap-less side of both particles

Figure 4a, b shows that the Sr mass distribution differs between the gap and the gap-less sides of the particles. For particle AGR2-223-RS34, the greatest mass is contained in the KP on the gap-less side of the particle, while for particle AGR2-223-RS06, the Sr mass in the KP is within error. Eu and Ba behave similarly (data not shown).

During irradiation the O:C ratio in the KP decreases relative to that in the kernel [6]. As Sr, Eu, and Ba are expected to form carbide phases [14], the increased C content appears to promote accumulation of these elements. Increased accumulation of presumed carbide phases on the non-gap side of the particle is also due to the fact that the KP on the gapless side tends to be thicker than the KP on the side with the gap [5]. The thicker KP on the gapless side provides a larger low-oxygen volume for presumed carbide phases to accumulate.

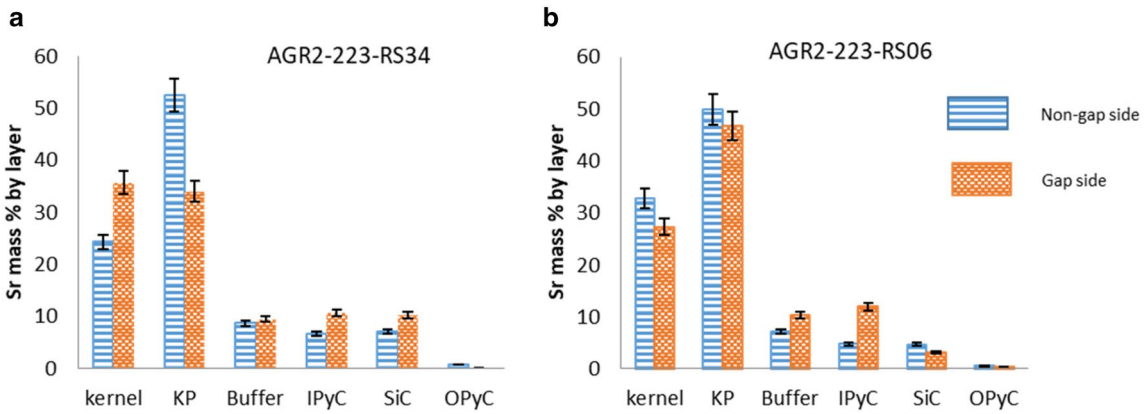

Fig. 4 **a**, **b** Shows Sr mass percentage as a fraction of the particle total Sr for the various layers on the gap and non-gap side of **a** AGR2-223-RS34 and **b** AGR2-223-RS06. 99% confidence interval error bars are shown. **a** is excerpted from [6]. 99% confidence interval error bars are shown

Enhanced fission product transport

The time-average, volume average (TAVA) temperature for compact AGR2-2-2-3 is 1261 °C. The TAVA temperature is the temperature experienced at centreline, which because it is an average, does not represent the actual temperature experienced by every particle. The temperature profile experienced by any particular particle in the same compact varies with the particle's position in the compact. Intra-particle compact positional differences can impart different temperatures and temperature gradients among the approximate 3176 particles that comprise the compact. As noted previously, AGR-2 compacts have an intra-compact temperature range of approximately 200 °C [9]; therefore, if higher temperatures are the only factor impacting Ag loss, particle AGR2-223-RS06 is expected to have experienced higher temperatures than particle AGR2-223-RS34.

Figure 3 demonstrates that for elements such as Cs, Sr, Pd and Ag, particle AGR2-223-RS34 shows enhanced transport relative to particle AGR2-223-RS06. It is difficult to reconcile apparent enhanced fission product transport in AGR2-223-RS34 relative to that of AGR2-223-RS06 when the former's high-Ag retention suggests that it was the colder particle. Some insight can be gained by the work of Lillo et al. [15] who noted differences in SiC layer grain boundaries between low-Ag retention particles and high-Ag retention particles. Specifically, they noted that high-Ag retention particles contain more twin-related grain boundaries than low-Ag retention particles, and that low-Ag retention particles contain a higher fraction of random, high-angle train boundaries, which are high diffusivity pathways. As they suspect that these differences arise during fabrication, it is possible that the high-Ag retention experienced by particle AGR2-223-RS34 is reflective of a different fabrication SiC microstructure than is present in AGR2-223-RS06. It is also possible that outward radial transport and release of Ag is controlled by different processes than those controlling the other fission products. According to Gerczak et al. [9], both particles retained a similar amount of ^{154}Eu (another mobile fission product), suggesting that this fission product does not behave like Ag. It is possible that other fission products in this study have transport properties that are more similar to Eu than Ag. More data are required to understand how Ag transport and retention differs from that of FPs such as Sr, Cs, and Pd.

The EPMA FP mass calculation closely correlates with the ORIGEN-model prediction for most FPs for both particles, suggesting the layer-specific masses for the well-correlated FPs are accurate; thus, FP behavioural differences between these two particles likely reflect positional differences within the compact. Such data can be used to better understand intra-compact variability and to improve FP transport modelling in TRISO particles.

Conclusions

- The EPMA-based mass balance technique compares favourably with ORIGEN-based FP mass predictions.
- Mass balance results show that Sr, Ba, and Eu accumulate in greater mass in the KP of the gap-less side of the particles when compared to the KP on the gap side of the particles.
- Mass balance results demonstrate that Cs, Sr, Pd, and Ag transport in particle AGR2-223-RS34 is enhanced compared with FP transport in particle AGR2-223-RS06.
- The high-Ag release from particle AGR2-223-RS06 compared to that of particle AGR2-223-RS34 appears to contradict the finding of enhanced fission product transport in the latter particle compared to the former. More data

are required to understand the factors influencing transport of the various fission products.

Acknowledgements We thank the National Scientific Users Facility (NSUF) for partial financial support. This work was sponsored by the U.S. Department of Energy, Office of Nuclear Energy, under U.S. Department of Energy Idaho Operations Office Contract DE-AC07-05ID14517. The United States Government retains and the publisher, by accepting the article for publication, acknowledges that the United States Government retains a nonexclusive, paid-up, irrevocable, worldwide license to publish or reproduce the published form of this manuscript, or allow others to do so, for United States Government purposes.

Data availability Data are available upon reasonable request from the corresponding author.

Declarations

Conflict of interest On behalf of the authors, there is no conflict of interest.

References

1. B. Collin, *AGR-2 Irradiation Test Final As-Run Report*, INL/EXT-14-32277 Rev. 3 (2018)
2. F. Rice, J. Stempien, P. Demkowicz, Nucl. Eng. Des. **329**, 73–81 (2018)
3. J. Stempien, M. Plummer, J. Schulthess, *Measurement of Kernel Swelling and Buffer Densification in Irradiated UCO and UO_2 TRISO Fuel Particles from AGR-2*, INL/EXT-19-54502 (2019)
4. S. Ploger, P. Demkowicz, J. Hunn, J. Kehn, Nucl. Eng. Des. **271**, 221–230 (2014)
5. I. Van Rooyen, Y. Yang, Z. Fu, B. Kombaiah, K. Wright, *Advanced Microscopy Report on UCO Fuel Kernels from Selected AGR-1 and AGR-2 Experiments*, Idaho National Laboratory External Report INL/EXT-21-00947 (2021)
6. K. Wright, J. Stempien, W. Jiang, I. van Rooyen, J. Nucl. Mater. **559**, 153468 (2022)
7. J.D. Hunn, T.J. Gerczak, R.N. Morris, C.A. Baldwin, F.C. Montgomery, 2016-2. PIE on safety-tested loose particles from compact 4-4-2. ORNL/TM-2015/16 (2016)
8. C.A. Baldwin, J.D. Hunn, R.N. Morris, F.C. Montgomery, C.M. Silva, P.A. Demkowicz, Nucl. Eng. Des. **271**, 131–141 (2014)
9. T.J. Gerczak, J.D. Hunn, R.N. Morris, F.C. Montgomery, D.J. Skitt, C.A. Baldwin, J.A. Dyer, B.D. Eckhart, Nucl. Eng. Des. **364**, 110656 (2020)
10. P. Demkowicz, J. Hunn, R. Morris, I. van Rooyen, T. Gerczak, J. Harp, S. Ploger, AGR-1 Post Irradiation Examination Final Report INL/EXT-15-36407 (2015)
11. J. Sterbentz, *JMOCUP As-Run Daily Depletion Calculation for the AGR-2 Experiment in the ATR B-12 Position*, Idaho National Laboratory ECAR-2066 (2014)
12. G. Hawkes, *AGR-2 Daily As-Run Thermal Analyses*, ECAR-2476, INL/MIS-14-31871 (2014)
13. G. Hawkes, *AGR-2 Irradiation Experiment Thermal Projections*, ECAR-1692 (2012)
14. F. Homan, T. Lindemer, E. Long Jr., T. Tiegs, R. Beatty, Nucl. Technol. **35**, 428 (1977)
15. T. Lillo, I. van Rooyen, J. Aguiar, Nucl. Eng. Des. **329**, 46–52 (2018)